

Template-Based Conformal Shape-from-Motion-and-Shading for Laparoscopy

Abed Malti, Adrien Bartoli, and Toby Collins

ALCoV-ISIT,
UMR 6284 CNRS/Université d'Auvergne,
28 Place Henri Dunant,
Clermont-Ferrand, France

<http://isit.u-clermont1.fr/~abed, ~ab, content/Toby-Collins>

Abstract. Shape-from-Shading (SfS) is one of the fundamental techniques to recover depth from a single view. Such a method has shown encouraging but limited results in laparoscopic surgery due to the complex reflectance properties of the organ tissues. On the other hand, Template-Based Deformable-Shape-from-Motion (DSfM) has been recently used to recover a coarse 3D shape in laparoscopy.

We propose to combine both geometric and photometric cues to robustly reconstruct 3D human organs. Our method is dubbed Deformable-Shape-from-Motion-and-Shading (DSfMS). It tackles the limits of classical SfS and DSfM methods: First the photometric template is reconstructed using rigid SfM (Shape-from-Motion) while the surgeon is exploring – but not deforming – the peritoneal environment. Second a rough 3D deformed shape is computed using a recent method for elastic surface from a single laparoscopic image. Third a fine 3D deformed shape is recovered using shading and specularities.

The proposed approach has been validated on both synthetic data and in-vivo laparoscopic videos of a uterus. Experimental results illustrate its effectiveness compared to SfS and DSfM.

1 Introduction

Over the past few years efforts have been made to develop systems for computer aided laparoscopy. It consists on helping the practitioners during the intervention to improve their perception of the intra-operative environment [10]. 3D sensing offers a virtual controllable view-point and is one of the major possible improvements to the current technology. However, due to the unpredictable, complex and elastic behaviour of living peritoneal tissues, 3D shape recovery from laparoscopic images is a difficult and open problem.

On the one hand, DSfM methods has shown effectiveness in recovering 3D shapes of elastic deformations in laparoscopy [17,7]. Based on how does the feature correspondences cover the surface, the 3D reconstruction can go from coarse to fine when the correspondences go from sparse to dense. Usually human organs are textureless and very specular which makes it difficult to densely cover the surface with feature correspondences using automatic feature detection and matching. On the other hand, SfS methods allow one to recover surface details. However, it is difficult to achieve remarkable 3D reconstructions due to the complex reflectance of the organ tissues. In addition, SfS does not allow one to solve temporal registration. In order to take advantage of these two methods and overcome their drawbacks, we propose to combine

them in a Deformable-Shape-from-Motion-and-Shading (DSfMS) framework. Figure 1 shows the effectiveness of our proposal when compared to SfS and DSfM: the shading cue provides details on the surface and the motion cue adds smoothness and global consistency.

Paper Organization. Section §2 presents state-of-the-art. Section §3 gives a geometric characterization of smooth surfaces. Section §4 presents the 3D template reconstruction. Section §5 gives a photometric reconstruction of the template albedo map. Section §6 recalls monocular conformal reconstruction. Section §7 presents monocular conformal reconstruction with shading cues. We finally report experimental results in section §8 and conclude. Our notation will be introduced throughout the paper.

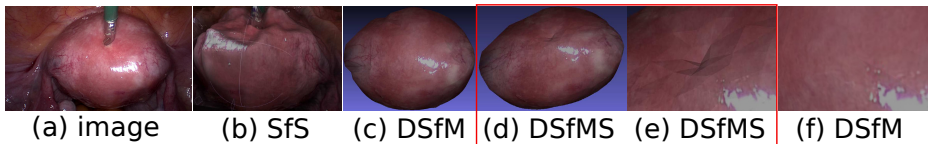


Fig. 1. Qualitative comparison between the proposed approach and previous methods. Using one Single input image with deformed organ from an in-vivo video sequence, the result of three reconstruction methods is shown. The reconstruction using classic SfS in figure (b) shows bumpy region. The reconstructions using DSfM and DSfMS in (c) and (d) show smoother results. An enlarged view of the deformed region allows us to observe in figure (e) that our DSfMS recovers the deformation while in figure (f) the DSfM recovers a coarse smooth surface.

2 Related Work

Intra-operative 3D sensing has recently gained a lot of interest in the field of laparoscopy. Various methods have been proposed that can be classified as active and passive. Active approaches consist of sensing techniques that modify the laparoscope’s hardware. In [5,6] an approach based on the detection of a laser beam line is described. The approach requires the insertion of two monocular endoscopes: one for the projection of the laser beam and one for observing the projected laser beam. In [12] a prototype of Time-of-Flight (ToF) endoscope is proposed and in [19] a set of incremental algorithms for 3D reconstruction has shown promising results using ToF endoscopes. Passive approaches consist of vision techniques based only on ‘regular’ images from the laparoscope. Both stereo and monocular endoscopes are concerned. In [17,3] methods based on disparity map computation for stereo-laparoscope have been proposed. Visual SLAM for dense surface reconstruction has been proposed in [18]. In the context of monocular laparoscopy, very few methods were proposed [2].

However, the computer vision community has made some effective achievements in the domain of template-based monocular 3D reconstruction of deformable surfaces. Using a template-based method provides a full geometric description of the surface rather than just a sparse or partially dense description as in the previously cited methods. This allows one to render the surface from a new viewpoint, recover self-occluded parts, and opens applications based on Augmented Reality. The problem of template-based

monocular 3D shape recovery is under-constrained because there is an infinite number of 3D surfaces that can project to the same image data. It is then of critical importance to constrain the problem to have a unique consistent solution or at least a small set of plausible solutions. Over the recent years, different types of physical and statistical constraints were proposed [8,15]. An important physical prior is isometry [1,13], which imposes that the geodesic distance is preserved by deformations. Recently a 3D conformal method has been proposed to reconstruct elastic deformations in the context of laparoscopy [7]. To provide good reconstruction results, SfM needs feature detection and matching in the deformed areas. The SfS problem is one of the eldest and fundamental problems in computer vision [23,14]. Recovering depths using shading cues has been extensively used for both rigid and deformable objects [23]. To provide good reconstruction results, SfS needs an estimation of the reflectance map of the reconstructed surface.

To overcome the bottleneck of SfS and DSfM, we can take advantage of both methods: using feature-based reconstruction to recover a deformed 3D surface and use shading cues to refine the reconstruction of areas which lack tracked features. This combined approach has been used in several other conditions to recover coarse to fine 3D shapes: For instance in rigid 3D reconstruction [22] presented an algorithm for computing optical flow, shape, motion, lighting, and albedo from an image sequence of a rigidly-moving Lambertian object under distant illumination. [20] proposed an approach to recover shape detail to dynamic scene geometry captured from multi-view video frames. [8] presented a closed-form solution to the problem of recovering the 3D shape of a non-rigid potentially stretchable surface from 3D-to-2D correspondences. In [16], a strategy for dense 3D depth recovery and temporal motion tracking for deformable surfaces using stereo-video sequence is proposed. It is worth to highlight that none of these methods were designed to combine SfS and DSfM for elastic surface reconstruction using one single view.

Contributions. The contribution of our work is three folds: (i) Combining SfS and DSfM, (ii) reconstruction of a template albedo map of in-vivo human organs and (iii) using shading cues to recover deformations in regions where feature correspondences are missing and using feature correspondences as boundary conditions to the reconstruction with shading.

3 Notation and Geometric Characterization of Smooth Surfaces

A smooth surface Γ can be parameterized by a \mathcal{C}^2 -function $\Phi: \Omega \subset \mathbb{R}^2 \rightarrow \mathbb{R}^3$: $(u, v) \mapsto \mathbf{Q} = (\Phi_x(u, v) \ \Phi_y(u, v) \ \Phi_z(u, v))^\top$. We do not make a distinction between the surface Γ and the mapping Φ unless needed. We call template the surface at rest.

The Jacobian of Φ , denoted J_Φ , is given by: $J_\Phi = \begin{pmatrix} \frac{\partial \Phi_x}{\partial u} & \frac{\partial \Phi_x}{\partial v} & \frac{\partial \Phi_x}{\partial v} \\ \frac{\partial \Phi_y}{\partial u} & \frac{\partial \Phi_y}{\partial v} & \frac{\partial \Phi_y}{\partial v} \\ \frac{\partial \Phi_z}{\partial u} & \frac{\partial \Phi_z}{\partial v} & \frac{\partial \Phi_z}{\partial v} \end{pmatrix}^\top$ It is a (3×2) matrix which at each $(u, v) \in \Omega$ maps a local unit square of Ω to a tangent plane at

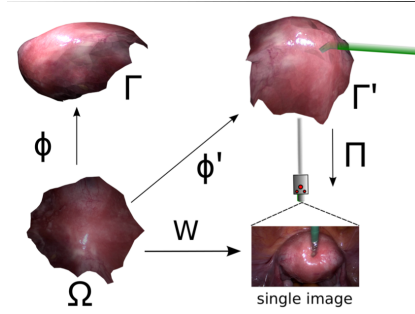


Fig. 2. Surface representation. Left: Φ is a conformal map. Geodesics on Ω , which is a flattening of Γ , are stretched on Γ . The angles tend to be preserved by Φ and area changes are tolerated. Φ' is the conformal map which reconstruct a deformation of the template Γ by the surgery tool. \mathcal{W} is correspondence function between the template and the deformed image. In our work, Φ is computed during the exploration phase. \mathcal{W} is computed from feature correspondences. Π is the projection matrix of a 3D point to the image plan including camera's intrinsics and Φ' is the unknown deformation function.

$\Phi(u, v)$. The normal of the surface at a point (u, v) is given by $\mathbf{N} = \left(\frac{\partial \Phi_x}{\partial u} \quad \frac{\partial \Phi_y}{\partial u} \quad \frac{\partial \Phi_z}{\partial u} \right)^\top \times \left(\frac{\partial \Phi_x}{\partial v} \quad \frac{\partial \Phi_y}{\partial v} \quad \frac{\partial \Phi_z}{\partial v} \right)^\top$. Where \times stands for the cross product in \mathbb{R}^3 . Let $\mathcal{W}: \Omega \rightarrow \mathbb{R}^2$ be a known warp which maps points from the template to surface points in the deformed image. The deformed image contains the projection of the deformed surface. In practice, \mathcal{W} can be a function which matches features in the template and in the deformed image. Let $\Pi: \mathbb{R}^3 \rightarrow \mathbb{R}^2: (x y z)^\top \mapsto (a b)^\top$ be the projection of a 3D point to the image plan.

4 Reconstruction of the Template's 3D Shape

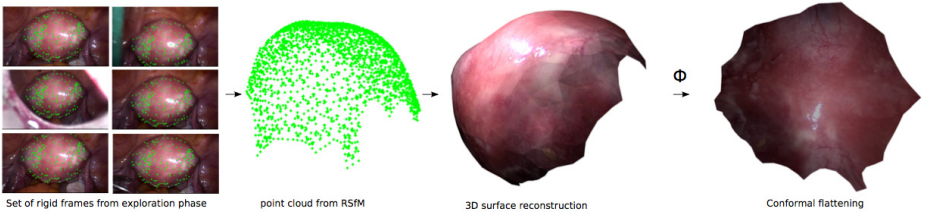


Fig. 3. Uterus template reconstruction during the exploration phase using a classic technique of Rigid SfM. From left-to-right: The rigid frames are combined to extract a dense point cloud of the uterus surface. Then, the 3D points are meshed and texture mapped. Finally, conformal flattening is applied.

As in [7], we assume that during the exploration of the peritoneal environment, the organs are at rest and the acquired image sequence undergoes a rigid motion of a rigid scene. This allows us to reconstruct both the template's 3D shape. From M views, Rigid SfM finds camera parameters as well as a set of 3D points $(x_j \ y_j \ z_j)$, $j = 1, \dots, N_v$ which will be the template points. There are several ways to proceed for Rigid SfM [4]. We chose the classical sequential approach where two different views with enough baseline are used to compute the essential matrix, from which the relative camera position can be extracted and used to triangulate a first set of 3D points. The camera position, T_i , $i = 1, \dots, M - 1$, for each other view is then computed on turn using camera resection, and new 3D points are triangulated. Finally, bundle adjustment is launched to minimize the reprojection error, and the 3D points are connected to form a mesh with N_F faces \mathcal{F} and N_v vertices \mathcal{V} given by the set of triangulated 3D points. Image consistent meshing can be used [9]. Conformal flattening can be used to estimate the geometric parameterization of the obtained surface. The results of applying this method to an in-vivo video sequence from laparosurgery is shown in figure 3.

5 Reconstruction of the Template's Albedo

Several methods were proposed to estimate the albedo of a surface [11,20]. In the context of laparosurgery, the light source is rigidly mounted on the tip of the endoscope and then can be assumed as being co-linear to the axis of the camera's principal axis $L = (0 \ 0 \ 1)^T$ (see figure 4). Assuming a Lambertian diffuse surface, the reflectance model expresses the image intensity at a pixel $\mathcal{W}(u, v)$ with respect to the surface normal $N(u, v)$ and the direction of the distant light source L : $\mathcal{I}(\mathcal{W}(u, v)) = \alpha(u, v)L \cot N(u, v)$, with $\alpha(u, v)$ is the albedo of the surface. Using the reconstructed template 3D surface the normals $N(u, v)$ can be easily computed. Given an image i , $i = 1, \dots, M$, the corresponding albedo map can be estimated as:

$$\alpha_i(u, v) = \frac{\mathcal{I}_i(u, v)}{L \cdot (R_i N(u, v))}, \quad i = 1, \dots, M \quad (1)$$

where R_i is the rotation part of T_i . This equation is not defined when L is perpendicular to $R_i N(u, v)$. This situation can be easily detected since both vectors are known and $\alpha_i(u, v)$ is set to a pre-defined maximum value. Another interesting situation is when the light source direction is parallel to the surface normal and then the full projected light is reflected by the surface toward the camera. Usually this effect saturates the camera sensor and the corresponding area appears as specular shining white in the image. We finally define the albedo map by computing the minimum value at each pixel over all frames. This process handles specularities and most of the other unmodeled effects:

$$\alpha(u, v) = \min_{i \in \{1, \dots, M\}} \alpha_i(u, v) \quad (2)$$

The obtained template's albedo of the in-vivo uterus sequence is displayed in figure 4.

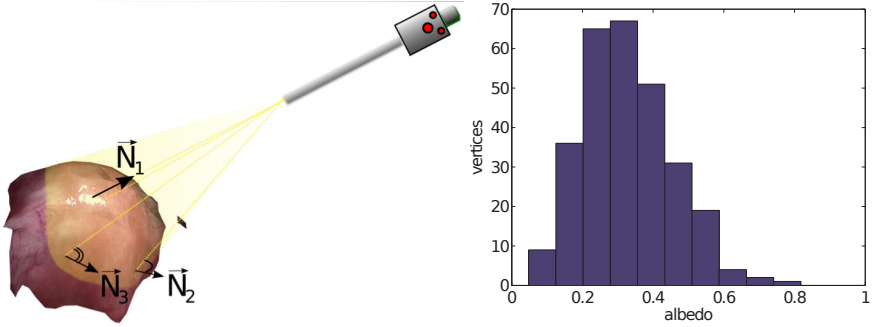


Fig. 4. Left: The image intensity at a surface point depends on the laparoscope’s light source direction and the surface normal at that point. Points which have a normal parallel to the light direction produce specularities in the resulting image. Right: The histogram values of the albedo of the vertices.

6 Monocular Conformal Reconstruction

In [7] a discrete conformal reconstruction of deformable surfaces is proposed from N_c point correspondences between the deformed shape in an image and the 3D template $\Phi(u_i, v_i) \leftrightarrow \mathcal{W}(u_i, v_i)$, $i = 1, \dots, N_c$. In the template, the correspondences are given by their barycentric coordinates $(f_i \mathbf{b}_i)^\top$, $i = 1, \dots, N_c$, relatively to the triangle they lie on. In the image, the correspondences are given in pixel coordinates $\mathcal{W}(u_i, v_i)^\top$, $i = 1, \dots, N_c$. Extensible 3D reconstruction was formulated in [7] as:

$$\begin{aligned}
 \min_{\mathcal{V}'} \sum_{i=1}^{N_c} & \| \Pi(\mathbf{K} \mathbf{v}'(f_i) \mathbf{b}_i) - \mathcal{W}(u_i, v_i) \| && \text{(motion)} \\
 + \lambda_1 \sum_{i=1}^{N_F} & \| \mathbf{S}_i - \mathbf{S}_i^0 \|^2 && \text{(shearing)} \\
 + \lambda_2 \sum_{i=1}^{N_F} & \| \mathbf{A}_i - \mathbf{A}_i^0 \|^2 && \text{(anisotropy)} \\
 + \lambda_3 \| \Delta \mathcal{V}' \|^2 & && \text{(smoothing)}
 \end{aligned} \tag{3}$$

where \mathbf{K} is the (3×3) intrinsic matrix of the camera, $\mathbf{v}'(f_i)$ is the (3×3) matrix whose columns are the 3D coordinates of the vertices of face i , \mathbf{S}_i and \mathbf{A}_i are the 2D shearing and anisotropy scaling transforms from the template to the deformed i^{th} face, λ_1 and λ_2 are two real positive weights that tune the importance of the shearing, the anisotropy scaling and the smoothing energy term. The combination of these two non-isometric transforms relaxes the inextensible condition and allows one to deal with local extensible deformations. \mathbf{S}^0 and \mathbf{A}^0 are average amounts of shearing and anisotropy for each face of the 3D template mesh. They can be either learned from training data or experimentally set. Practically, normalized shearing and anisotropy transforms are experimentally set and then scaled by the triangle area of each face f_i to obtain the transforms \mathbf{S}_i^0 and \mathbf{A}_i^0 . The additional weighted energy term smoothes the deformed shape. It is expressed through the linear Laplace-Beltrami discrete linear operator Δ of dimension $N_v \times N_v$ [21]. \mathcal{V}' is an $N_v \times 3$ matrix which concatenates the 3D mesh vertices \mathcal{V}'_i of the reconstructed deformed mesh. This result is used as input to our monocular DSfMS method.

7 Monocular Conformal DSfMS

The resulting deformed shape with the set of vertices $\mathcal{V}'_i, i = 1, \dots, N_v$, recovered from the previously described method can be refined using shading cues. Using the reconstructed template albedo values $\alpha(u_i, v_i), i = 1, \dots, N_v$ for each vertex, we formulate the conformal reconstruction with motion and shading cues reconstruction as:

$$\begin{aligned}
 \min_{\mathcal{V}''} \sum_{i=1}^{N_c} & \left\| (0 \ 0 \ 1)^\top \mathbf{v}''(f_i) \begin{pmatrix} b_{1i} \\ b_{2i} \\ b_{3i} \end{pmatrix} - (0 \ 0 \ 1)^\top \mathbf{v}'(f_i) \begin{pmatrix} b_{1i} \\ b_{2i} \\ b_{3i} \end{pmatrix} \right\| + & \text{(boundary cond.)} \\
 \lambda_4 \sum_{i=1}^N & \left\| \Pi(\mathbf{K}\mathbf{v}''_i) - \Pi(\mathbf{K}\mathbf{v}'_i) \right\|^2 + & \text{(reprojection cond.)} \\
 \lambda_5 \sum_{i \in \mathcal{D}_v} & \left\| \mathcal{I}'(\mathcal{W}''(u_i, v_i)) - \alpha(u_i, v_i) \mathbf{L} \cdot \mathbf{N}''(u_i, v_i) \right\|^2 + & \text{(diffuse vertices)} \\
 \lambda_6 \sum_{i \in \mathcal{S}_v} & \left\| \mathbf{L} \times \mathbf{N}''(u_i, v_i) \right\|^2 + & \text{(specular vertices)} \\
 \lambda_7 & \left\| \Delta \mathcal{V}'' \right\|^2 & \text{(smoothing)}
 \end{aligned} \tag{4}$$

where \mathcal{D}_v and \mathcal{S}_v are respectively the diffuse and specular vertices. The specular vertices can be easily detected as saturated regions in the deformed image intensity \mathcal{I}' . The real parameters $\lambda_4, \lambda_5, \lambda_6, \lambda_7$ are experimentally set. Through the boundary condition, this formulation gives confidence to the depth of the correspondences reconstructed by the conformal method using motion. The reprojection condition limits the refinement of the vertices along the camera sightlines. The diffuse condition refines the diffuse vertices according to the Lambertian model using shading. The specular vertices are constrained to have their normals parallel to the direction of the source light. Due to noise in the image intensity a smoothing term is needed to avoid bumpy surface reconstructions. The diffuse and specular terms allows us to recover the deformed surface in regions where the data correspondences are missing.

8 Experimental Results

8.1 Synthetic Data

The synthetic deformation model. The obtained template mesh is deformed to evaluate the performance of our approach with different amounts of edge extension and curvature changes. The synthetic deformation model enables us to simulate a push and pull by the surgeon's tool upon the uterus tissue. It is defined as a set of pairs of unit vectors \mathbf{F}_j and attraction points $\mathbf{g}_j: \{(\mathbf{F}_j, \mathbf{g}_j)\}_{j \in J}, J = \{1, \dots, d\}$. \mathbf{F}_j represents the main direction of deformation toward the attraction point \mathbf{g}_j and d is the number of attraction points. Given a pair $(\mathbf{F}_j, \mathbf{g}_j)$, the new location of a vertex of the template mesh is computed as: $\overrightarrow{\mathbf{v}_i \mathbf{v}'_i} = k((\mathbf{F}_j, \overrightarrow{\mathbf{v}_i \mathbf{g}_j})) \overrightarrow{\mathbf{v}_i \mathbf{g}_j} + \epsilon \mathbf{N}_i$, where \mathbf{N}_i is the unit normal of the surface at the point \mathbf{v}_i , ϵ is a real number of small value used to move the vertex according to the tangent plan and avoid to drag it abruptly toward the attraction point. k is a function which models the effect of the attraction between \mathbf{g}_j and \mathbf{v}_i . It is assumed to be dependent only on the angle between the main direction of deformation and the vector joining the vertex to the attraction point. The smaller this angle the bigger the effect of the attraction point on the vertex.

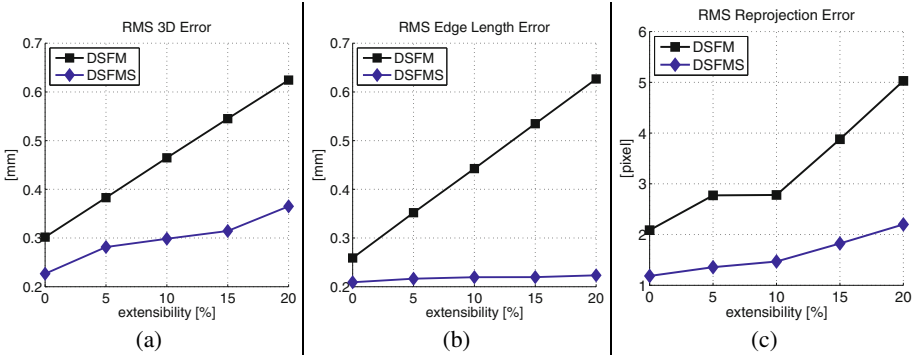


Fig. 5. 3D reconstruction error versus extensibility for conformal DSfM and DSfMS methods using the synthetic sequence *ext*







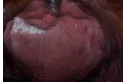

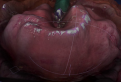
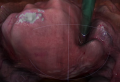
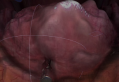
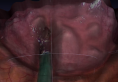
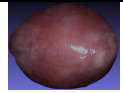
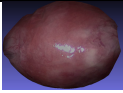
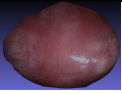
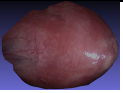
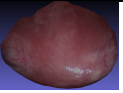
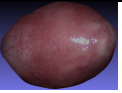
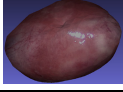
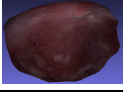
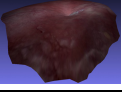
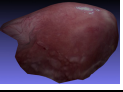
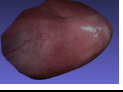
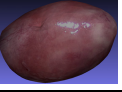
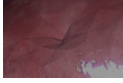
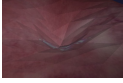
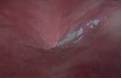

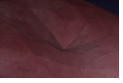
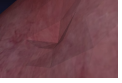
Results. A sequence of 500 deformations is produced so that the amount of extensibility *w.r.t.* the template varies as: $ext = [0\% \ 5\% \ 10\% \ 15\% \ 20\%]$. The deformed images are obtained by projecting each 3D deformed mesh using a perspective projection matrix Π . The intrinsics of this projection are taken as being the same as a Karl Storz laparoscope’s intrinsics. A z-buffer rendering method is used to compute the self-occluded areas and to texture map the projected mesh. The point correspondences are from the 3D template mesh to 2D deformed image. They are obtained by randomly choosing 500 points represented by their barycentric coordinates. In the deformed mesh the points, which have the same barycentric coordinates, are projected using the same perspective projection matrix Π to obtain the 2D correspondences in the deformed image. We proceed to the evaluation of the developed method by adding Gaussian noise of zero mean and different variances to the 2D correspondences. Since in real in-vivo video sequence it is very difficult to automatically obtain correspondences in the deformed area due to the presence of the surgery tool and moving specularities, we do not consider any synthetic correspondences in the deformed area. Only 25 point correspondences are used between the 3D template and the 2D single input image. For lack of space, the qualitative reconstructed surface are not shown for DSfM and DSfMS. The quantitative results show the RMS 3D error of vertices is computed as the summed norm of the difference between reconstructed and ground truth vertices. The RMS edge length error is computed as the summed norm of difference of the mesh edge’s lengths between reconstructed and ground truth surface. The reprojection error is computed as the summed norm of difference between the projection of the points in the reconstructed mesh and the corresponding in the deformed image. As expected, in the case of sparse feature correspondences, the DSfMS outperforms the DSfM method. When the number of correspondences is augmented in the deformed regions, the DSfM method tends to be as accurate as the proposed method.

8.2 Real Data

To validate the proposed approach on real data, the experiment we propose is the 3D reconstruction of an uterus from in-vivo sequences acquired using a monocular Karl

Storz laparoscope. The 3D template of the uterus is generated during the laparosurgery exploration step of the inside body. Then, a set of complex and unpredictable deformations may occur on the uterus when the surgeon starts to examine it. A set of 35 correspondences between the 3D uterus template and the deformed images was generated. The correspondences in deformed regions are either absent or non-stable and then are not taken into account. As it is hard to provide ground truth data to compare with, besides the quantitative results from the synthetic data, the qualitative 3D reconstruction shows clear improvement of the recovery of the deformed region with no need of point correspondences. Table 1 compares 3D reconstructed deformation with SfS, DSfM and the proposed DSfMS. As expected, the SfS method provide bumpy reconstructed surface due to specularities and unmodeled physical phenomena. The DSfM method provides coarse reconstruction since feature correspondences are missing in the deformed regions. DSfMS provides a finer and meaningful 3D reconstruction.

Table 1. 3D reconstruction on in-vivo video sequence from monocular laparoscope using SfS, DSfM and the proposed DSfMS. First row: Single 2D views of uterus deformation with a surgery tool. Second row: 3D reconstruction using SfS. Each 3D reconstruction is done using the single view above. The view is given in the laparoscope view point. Third row: 3D deformed surface seen from different point of view which provide visualization of the self-occluded part. Fourth row: Zoom in the deformed reconstructed area with DSfMS.

Single image						
Classic SfS						
DSfM with few corresp.						
DSfMS with few corresp						
Zoom (DSfMS)						

9 Conclusion

In this paper, we have presented the DSfMS method to reconstruct a conformal deforming living tissue in 3D by combining motion and shading cues. Our method provides novel technical contributions and also a new way of tackling the 3D vision problem in laparoscopy. The synthetic data and in-vivo experimental results show the ability of the proposed method to recover a smooth surface subjected to deformation in local region without correspondences.

References

1. Brunet, F., Hartley, R., Bartoli, A., Navab, N., Malgouyres, R.: Monocular Template-Based Reconstruction of Smooth and Inextensible Surfaces. In: Kimmel, R., Klette, R., Sugimoto, A. (eds.) ACCV 2010, Part III. LNCS, vol. 6494, pp. 52–66. Springer, Heidelberg (2011)
2. Grasa, O.G., Civera, J., Montiel, J.: EKF monocular slam with relocalization for laparoscopic sequences. In: ICRA (2011)
3. Hager, G., Vagvolgyi, B., Yuh, D.: Stereoscopic video overlay with deformable registration. *Medicine Meets Virtual Reality* (2007)
4. Hartley, R.I., Zisserman, A.: *Multiple View Geometry in Computer Vision*, 2nd edn. Cambridge University Press (2003)
5. Hayashibe, M., Suzuki, N., Hattori, A., Nakamura, Y.: Intraoperative Fast 3D Shape Recovery of Abdominal Organs in Laparoscopy. In: Dohi, T., Kikinis, R. (eds.) MICCAI 2002. LNCS, vol. 2489, pp. 356–363. Springer, Heidelberg (2002)
6. Hayashibe, M., Suzuki, N., Nakamura, Y.: Laser-scan endoscope system for intraoperative-geometry acquisition and surgical robot safety management. *MIA* 10, 509–519 (2006)
7. Malti, A., Bartoli, A., Collins, T.: Template-based conformal shape-from-motion from registered laparoscopic images. In: MIUA (2011)
8. Moreno-Noguer, F., Salzmann, M., Lepetit, V., Fua, P.: Capturing 3D stretchable surfaces from single images in closed form. In: CVPR (2009)
9. Morris, D.D., Kanade, T.: Image-consistent surface triangulation. In: CVPR (2000)
10. Nicolau, S.A., Pennec, X., Soler, L., Ayache, N.: A Complete Augmented Reality Guidance System for Liver Punctures: First Clinical Evaluation. In: Duncan, J.S., Gerig, G. (eds.) MICCAI 2005. LNCS, vol. 3749, pp. 539–547. Springer, Heidelberg (2005)
11. Nishino, K., Zhang, Z., Ikeuchi, K.: Illumination distribution from a sparse set of images for view-dependent image synthesis. In: ICCV (2001)
12. Penne, J., Höller, K., Stürmer, M., Schrauder, T., Schneider, A., Engelbrecht, R., Feußner, H., Schmauss, B., Hornegger, J.: Time-of-Flight 3-D Endoscopy. In: Yang, G.-Z., Hawkes, D., Rueckert, D., Noble, A., Taylor, C. (eds.) MICCAI 2009. LNCS, vol. 5761, pp. 467–474. Springer, Heidelberg (2009)
13. Perriollat, M., Hartley, R., Bartoli, A.: Monocular template-based reconstruction of inextensible surfaces. In: BMVC (2008)
14. Prados, E., Camilli, F., Faugeras, O.: A unifying and rigorous shape from shading method adapted to realistic data and applications. *Journal of Mathematical Imaging and Vision* 25(3), 307–328 (2006)
15. Salzmann, M., Urtasun, R., Fua, P.: Local deformation models for monocular 3D shape recovery. In: CVPR (2008)
16. Stoyanov, D., Darzi, A., Yang, G.-Z.: Dense 3D Depth Recovery for Soft Tissue Deformation During Robotically Assisted Laparoscopic Surgery. In: Barillot, C., Haynor, D.R., Hellier, P. (eds.) MICCAI 2004. LNCS, vol. 3217, pp. 41–48. Springer, Heidelberg (2004)
17. Stoyanov, D., Scarzanella, M.V., Pratt, P., Yang, G.-Z.: Real-Time Stereo Reconstruction in Robotically Assisted Minimally Invasive Surgery. In: Jiang, T., et al. (eds.) MICCAI 2010, Part I. LNCS, vol. 6361, pp. 275–282. Springer, Heidelberg (2010)
18. Totz, J., Mountney, P., Stoyanov, D., Yang, G.-Z.: Dense Surface Reconstruction for Enhanced Navigation in MIS. In: Fichtinger, G., Martel, A., Peters, T. (eds.) MICCAI 2011, Part I. LNCS, vol. 6891, pp. 89–96. Springer, Heidelberg (2011)
19. Winter, M.: Image-Based Incremental Reconstruction, Rendering and Augmented Visualization of Surfaces for Endoscopic Surgery. PhD thesis, University of Erlangen (2009)
20. Wu, C., Varanasi, K., Liu, Y., Seidel, H.-P., Theobalt, C.: Shading-based dynamic shape refinement from multi-view video under general illumination. In: ICCV (2011)
21. Yoo, D.: Three-dimensional morphing of similar shapes using a template mesh. *International Journal of Precision Engineering and Manufacturing* (2009)
22. Zhang, L., Curless, B., Hertzmann, A., Seitz, S.M.: Shape and motion under varying illumination: Unifying structure from motion, photometric stereo, and multi-view stereo. In: ICCV (2003)
23. Zhang, R., Tsai, P.-S., Cryer, J.E., Shah, M.: Shape from shading: A survey. *PAMI* 21(8), 690–706 (1999)